frontiers | Frontiers in Marine Science

TYPE Original Research
PUBLISHED 26 October 2023
DOI 10.3389/fmars.2023.1285426

OPEN ACCESS

EDITED BY
Pengfei Xue,
Michigan Technological University,
United States

REVIEWED BY
Fajin Chen,
Guangdong Ocean University, China
Xing Zhou,
Georgia Institute of Technology,
United States

*CORRESPONDENCE
Wenxia Zhang
wenxiazhang1986@126.com;
zhangwx@sio.org.cn

RECEIVED 29 August 2023
ACCEPTED 13 October 2023
PUBLISHED 26 October 2023

CITATION
Wu H, Yang W, Zhang W and Zhao X (2023) Changjiang and Kuroshio contributions to oxygen depletion on the Zhejiang Coast. *Front. Mar. Sci.* 10:1285426. doi: 10.3389/fmars.2023.1285426

Changjiang and Kuroshio contributions to oxygen depletion on the Zhejiang Coast

Haokun Wu[1], Wen Yang[1], Wenxia Zhang[2,3]* and Xin Zhao[2]

[1]State Key Laboratory of Estuarine and Coastal Research, East China Normal University, Shanghai, China, [2]Key Laboratory of Ocean Space Resource Management Technology, Ministry of Natural Resources, Hangzhou, China, [3]State Key Laboratory of Satellite Ocean Environment Dynamics, Second Institute of Oceanography, Ministry of Natural Resources, Hangzhou, China

In recent decades, intensified anthropogenic activities have resulted in increasing occurrence of hypoxia in the East China Sea. Kuroshio, as a natural factor, also threatens the oxygen content over the continental shelf. There have been many studies investigating the different contributions of Changjiang and Kuroshio to oxygen depletion over the continental shelf. This study revisited this issue and further investigated the mechanisms controlling the different role of Changjiang and Kuroshio in oxygen depletion and focused mainly on the Zhejiang Coast. A coupled high-resolution physical-biogeochemical model was used to investigate the connections between the variations in nutrients, chlorophyll, stratification, and oxygen and the delivery of Changjiang diluted water and Kuroshio subsurface water over the shelf, especially on the Zhejiang Coast in the summer of 2017. The distinct features of hypoxia off the Changjiang estuary (severe but transient) and that along the Zhejiang Coast (mild but prolonged) are caused by the different dynamic environments and nutrients sources. North of 30°N, intense oxygen depletion and bottom hypoxia are typically under the constraint of Changjiang diluted water. While the impacts of upwelled materials associated with the Kuroshio subsurface water enhance southward with the simultaneously weakened impacts from the Changjiang diluted water. Besides confirming the support of upwelling on surface phytoplankton bloom along the Zhejiang Coast, this study detected subsurface chlorophyll maximum immediately underneath the main pycnocline offshore of the Zhejiang Coast during upwelling. This indicated that the upwelled oceanic nutrients were transported further offshore along isopycnals and also fertilized phytoplankton growth at the subsurface. The exacerbation of either anthropogenic or natural factors could potentially intensify oxygen depletion along the Zhejiang Coast.

KEYWORDS

coastal hypoxia, Changjiang, Kuroshio, upwelling, coupled physicalbiogeochemical model, Zhejiang coast

1 Introduction

Hypoxia, defined as dissolved oxygen concentration in seawater below 2 $mg{\cdot}L^{-1}$ or 62.5 $mmol{\cdot}m^{-3}$, has been rapidly increasing in recent years due to frequent human activities in coastal areas (Levin et al., 2009; Breitburg et al., 2018; Fennel and Laurent, 2018; Jarvis et al., 2021). Dissolved oxygen plays an indispensable role in sustaining marine organisms, and its depletion poses a considerable threat to the marine ecosystem, resulting in habitat destruction, reduced biodiversity, and even mortality (Diaz and Rosenberg, 2008; Zhang et al., 2010; Zhang et al., 2013). The increasing frequency and the detrimental effects of hypoxia have drawn extensive attention from researchers and stakeholders.

Over the past few decades, hypoxia has frequently occurred in the East China Sea (Chen et al., 2007; Wei et al., 2017). The dissolved oxygen concentration in the East China Sea had exhibited a pronounced decline trend over time (Wang, 2009; Ning et al., 2011), and the extent of hypoxia exceeded 15000 km^2 (Zhu et al., 2017). Due to significant differences in the spatial development of oxygen depletion, the hypoxic zone can be divided into two parts: the northern region (off the Changjiang estuary) and the southern region (along the Zhejiang Coast) (Wang et al., 2012; Chi et al., 2020). Changjiang strongly influences hypoxia formation and sustainment in the northern region (Rabouille et al., 2008; Liu et al., 2015; Zhou et al., 2017). The northern region bottom hypoxia is severe, but its duration is generally short due to the mobile spatial distribution of Changjiang diluted water (Zhang et al., 2018). On the other hand, oxygen depletion in the southern region is more moderate but longer-lived under the persistent influence from the intrusion of Kuroshio subsurface water (Zhu et al., 2011). With the presence of multiple water masses (i.e., Changjiang diluted water, continental shelf water, and Kuroshio water) (Chen, 2009), the hydrological environment and nutrient dynamic of the East China Sea is complex (Gong et al., 1996; Liu et al., 2021).

Changjiang is the primary terrestrial source of the East China Sea (Tong et al., 2015), forming a buoyancy plume called Changjiang diluted water by the mixing of riverine freshwater and continental shelf water (Chang and Isobe, 2003). The Changjiang diluted water predominantly expands northeast in summer under the East Asian Monsoon (Isobe et al., 2002), with a portion being transported to the Zhejiang Coast as the southern branch (Lie et al., 2003). The riverine inputs of freshwater and anthropogenic nutrients enhance water column stratification and stimulate phytoplankton blooms, promoting subsurface oxygen depletion and even resulting in severe hypoxia (Wei et al., 2007; Zhou et al., 2017; Liblik et al., 2020; Zhang et al., 2021). Therefore, regions with substantial riverine inputs may be particularly vulnerable to hypoxia.

Kuroshio subsurface water intrudes onto the continental shelf of the East China Sea (Chen, 2009), and also significantly impacts the shelf processes (Zhang et al., 2007; Yang et al., 2018). The southward Changjiang diluted water, the shelf water, and the northward Kuroshio intrusion confluence along the Zhejiang Coast, and interact with one another. The meeting of different water masses with large density differences induces horizontal density gradients and forces frontogenesis. The density front is maintained by strong tidal mixing and subsequently triggers the formation of upwelling (Zhu, 2003; Lü et al., 2006; Lü et al., 2007). As an essential pathway for Kuroshio affecting the upper layer, coastal upwelling introduces subsurface nutrient-rich water to the euphotic layer, elevating the phytoplankton biomass (Chen et al., 2004; Chen et al., 2021). Although the concentration of oceanic nutrients from Kuroshio is much lower compared to that of riverine nutrients, the northward intrusion of Kuroshio subsurface water persistently provides nutrients to the East China Sea (Chen, 1996; Chen and Wang, 1999; Yang et al., 2013). Oceanic nutrients fuel the growth of phytoplankton and play an important role in the development of hypoxia (Wang et al., 2016; Große et al., 2020; Xu et al., 2020; Tian et al., 2022). Wei et al. (2021) used *in-situ* observation to explore the effects of river plumes and coastal upwelling on oxygen depletion along the Zhejiang Coast.

Investigations based on traditional *in-situ* observations are usually constrained by limited temporal and spatial resolution. Numerical models can serve as a cost-effective and practical tool to investigate oxygen depletion processes, particularly when attempting to capture fine-scale variations. Meng et al. (2020) found that the supply of nutrients by vertical advection stimulated the phytoplankton growth in the southern East China Sea. Luo et al. (2023) pointed out that the transport of oceanic nutrients was affected by upwelling, regulating the primary production over the inner shelf. Große et al. (2020) tracked different nutrient sources in a 3-D model and quantified the contributions of riverine and oceanic nutrients to hypoxia formation over the shelf. Zhou et al. (2017) and Tian et al. (2022) suggest that the hypoxia extent in the East China Sea was regulated by both riverine and oceanic nutrients. Zhang et al. (2021) also suggested that nutrients from Changjiang and Kuroshio both regulate the hypoxia extent and chlorophyll content over the East China Sea. To advance the existing findings, this study explores the mechanisms of contributions of Changjiang and Kuroshio to oxygen depletion in different regions over the continental shelf. Six-hour model data for July 2017, a time period with no typhoon affecting the shelf, was analyzed to avoid the intense distraction of extreme events on dissolved oxygen dynamics. First, we described the main hydrological and biochemical characteristics in the study area (Figure 1). Then, we analyzed the time series of variables and linked the variations in nutrients, chlorophyll, and oxygen with the delivery of Changjiang diluted water and Kuroshio subsurface water to discuss the reasons of the spatially different effects of Changjiang and Kuroshio on oxygen depletion. The time continuum and inventory (depth-integration) of chlorophyll imply that the delivery of oceanic nutrients via upwelling also temporally relieves the nutrients limiting of subsurface phytoplankton growth for the offshore region along the Zhejiang Coast.

2 Methodology

2.1 Model description

We used the Regional Ocean Modeling System (ROMS) (Shchepetkin and McWilliams, 2005) hydrodynamic model

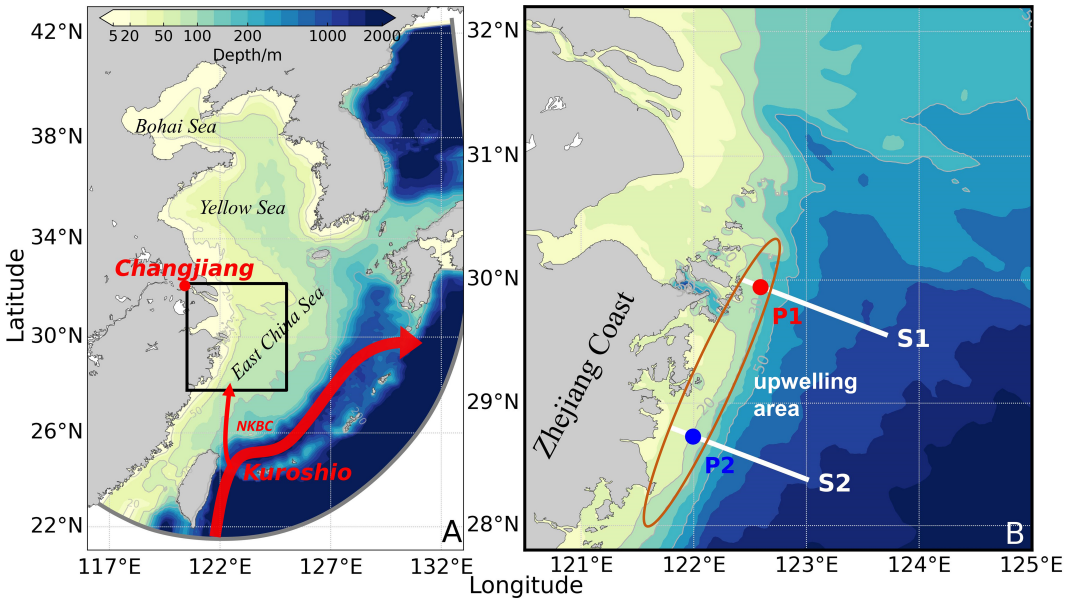

FIGURE 1
The model area **(A)** and the study area **(B)**. In panel **(A)**, the red dot indicates the location of Changjiang in the model, the thick red arrow indicates the paths of Kuroshio, the thin red arrow indicates the paths of nearshore Kuroshio branch current (NKBC), and the black rectangle indicates the location of the study area in the model area. In panel **(B)**, the white lines indicate the locations of sections S1 and S2, the red and blue dots indicate the locations of sites P1 and P2, respectively, and the brown ellipse roughly marks the upwelling area of the Zhejiang Coast.

coupled with a biogeochemical model. The hydrodynamic model domain is the same as Zhang et al. (2018), which encompasses the entire Bohai Sea, Yellow Sea, East China Sea, part of the Japan Sea and deep region offshore (Figure 1A). This ROMS-based model has 30 vertical layers, with a minimum water depth of 3 m and a maximum depth of slightly greater than 7000 m. The horizontal resolution ranges from around 500 m in the upper estuary, to ~1 km in the plume near-field region, and to ~2 km in the offshore region. The model run was initiated from rest and was forced with surface momentum and heat fluxes from the ERA5 dataset provided by the European Center for Medium-Range Weather Forecasts (ECMWF, https://www.ecmwf.int/en/forecasts/datasets), freshwater flux of Changjiang that obtained from Datong gauging station, and current and tide at the open boundary. The initial and open boundary conditions for physical components are extracted from the daily Hybrid Coordinate Ocean Model (HYCOM, https://www.hycom.org/dataserver). Thirteen tidal constituents (MM, MF, Q1, O1, P1, K1, N2, M2, S2, K2, MN4, M4, and MS4) are imposed based on tidal elevations and currents extracted from the global inverse tide model TPXO7.2 of Oregon State University (Egbert and Erofeeva, 2002).

The biogeochemical component is a simplified nitrogen cycle model (Fennel et al., 2006) that expanded to include the dynamics of DIP (Dissolved Inorganic Phosphorus) (Laurent et al., 2017) (Figure 2). A mass-conserving sediment oxygen demand was specified following Fennel et al. (2006), which assumes all sinking (aquatic phytoplankton-derived) oceanic organic matter that reaches the water-sediment interface is remineralized instantaneously. This sediment treatment consumes dissolved oxygen and releases NH_4 and PO_4 to the bottom water, and a portion of the organic nitrogen is lost to nitrogen gas (N_2) *via* denitrification. The same biogeochemical model scheme has been successfully applied and shown satisfying performance in other hypoxic regions, including the northern Gulf of Mexico and the Chesapeake Bay (Fennel et al., 2013; Feng et al., 2015). The initial and open boundary conditions for nutrients and oxygen were extracted from the climatological monthly World Ocean Atlas 2013 (WOA13, https://www.nodc.noaa.gov/OC5/woa13/). A full description of the model setup is provided by Zhang et al. (2018) and Zhang (2022a).

This coupled model has been previously validated to be in good agreement with the observed data for temperature, salinity, bottom dissolved oxygen, and surface chlorophyll (Zhang et al., 2018; Zhang et al., 2019; Zhang et al., 2021). Readers can refer to Zhang et al. (2018) and Zhang (2022a) for a detailed description of the model setup and parameter selections. This model has been used to investigate oxygen dynamics off the Changjiang estuary and factors controlling the short-timescale spatiotemporal spread of seasonal hypoxia off the estuary (Zhang et al., 2018; Zhang et al., 2022b). In this study, the model was initiated in January 2015 and ran for 3 years, with the first two years for sufficient spin-up. Strong wind like typhoons can disrupt bottom hypoxia (Zhang et al., 2020). There were no typhoons passing through the Changjiang estuary in July 2017. Thus, no strong wind events (typhoons) would affect the oxygen dynamics in July 2017, which is required for our investigation on a continuous time scale. For this reason, we focused on the status in 2017. The *in-situ* observation data collected in July 2017 were used to validate the model

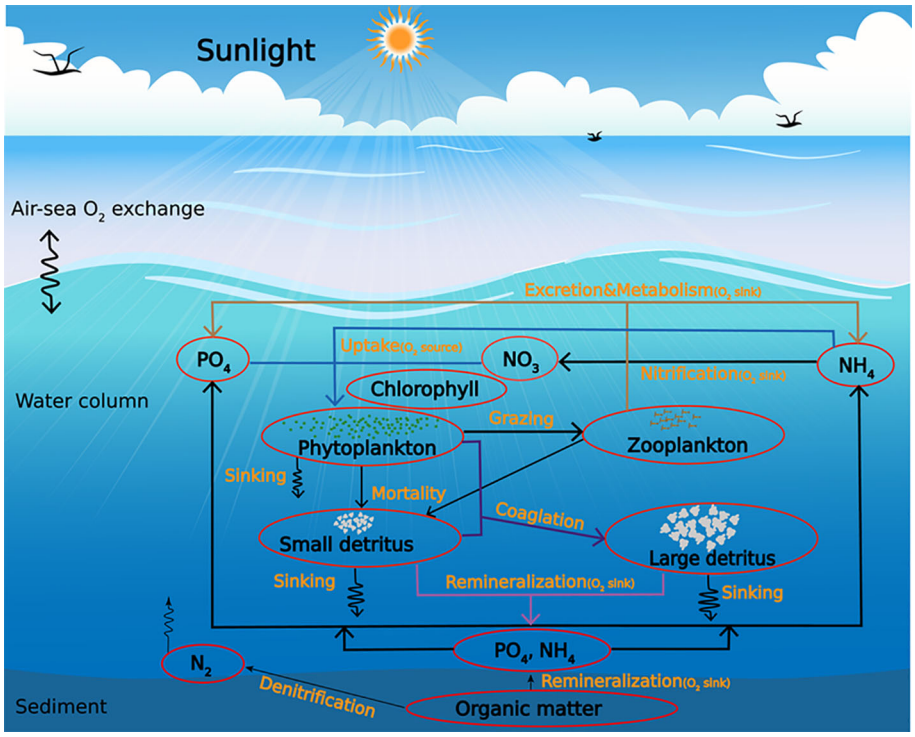

FIGURE 2
The biogeochemical model is represented by a schematic that illustrates the ecological processes and pathways. The model marks the biogeochemical processes that generate and consume dissolved oxygen (O_2), which are denoted as an O_2 source and sink, respectively. Note that this figure was modified based on Zhang (2022a).

performance for temperature, salinity, and dissolved oxygen (RMSEs of 2.66, 5.08, and 64.99, respectively) (Figure 3). The model performance is decent, and the analysis of dynamical and biological processes in the Changjiang estuary region based on this model is reliable.

2.2 Data analysis

In this study, we utilized the difference in density between the surface and bottom to simply represent the strength of vertical stratification. In addition, we used the maximum vertical gradients of density and dissolved oxygen at the sites to represent the pycnocline and oxycline. The gradient method was also used to calculate the bottom salinity front for front detection (Huang et al., 2010; He et al., 2016). The model grids were firstly interpolated into the orthogonal grids, and then the salinity gradient was calculated for all 3 × 3 grids using Equation (1).

$$Salinity\ Gradient = \sqrt{\left(\frac{\Delta S_1}{\Delta X_1}\right)^2 + \left(\frac{\Delta S_2}{\Delta X_2}\right)^2} \quad (1)$$

where ΔS_1 and ΔS_2 are salinity differences along the diagonal of all 3 × 3 grids, and ΔX_1 and ΔX_2 are the distance between the diagonals. The grid is considered to be located in the frontal zone when the salinity gradient is greater than 10 times the average salinity gradient in the study area (Fedorov, 1986).

3 Results

3.1 Hydrological environment and chlorophyll distribution

The evolutions of the distribution of surface temperature, salinity, chlorophyll, and depth-integrated chlorophyll in the study area in July 2017 were checked (Figure 4). Low-temperature patches (dark blue areas, Figures 4A-D) were seen along the Zhejiang Coast with significant surface temperature variations compared to the surrounding water (Figures 4A-D). The low-temperature patches gradually shrank and almost disappeared on July 20. Previous studies suggested that upwelling uplifted subsurface cold water to cool the surface water forming low-temperature patches (Lü et al., 2010), which was an essential way for Kuroshio intrusion to affect the inner shelf (Yang et al., 2013). The extent of low-temperature patches evolved over time, so four specific periods (July 6, 10, 15, and 20) were selected to investigate the evolution of the effects of upwelling and Kuroshio in the study area.

Surface salinity was utilized to investigate the distribution of Changjiang diluted water by using 31 isohalines (white isolines in Figures 4E-H) (Zhang et al., 2018). On July 6, the surface low-salinity water (salinity less than 31) was primarily concentrated off the Changjiang estuary, and a small portion of low-salinity water flowed southward (Figure 4E). During this period, the southern branch of the Changjiang diluted water covered sites P1 and P2 (red

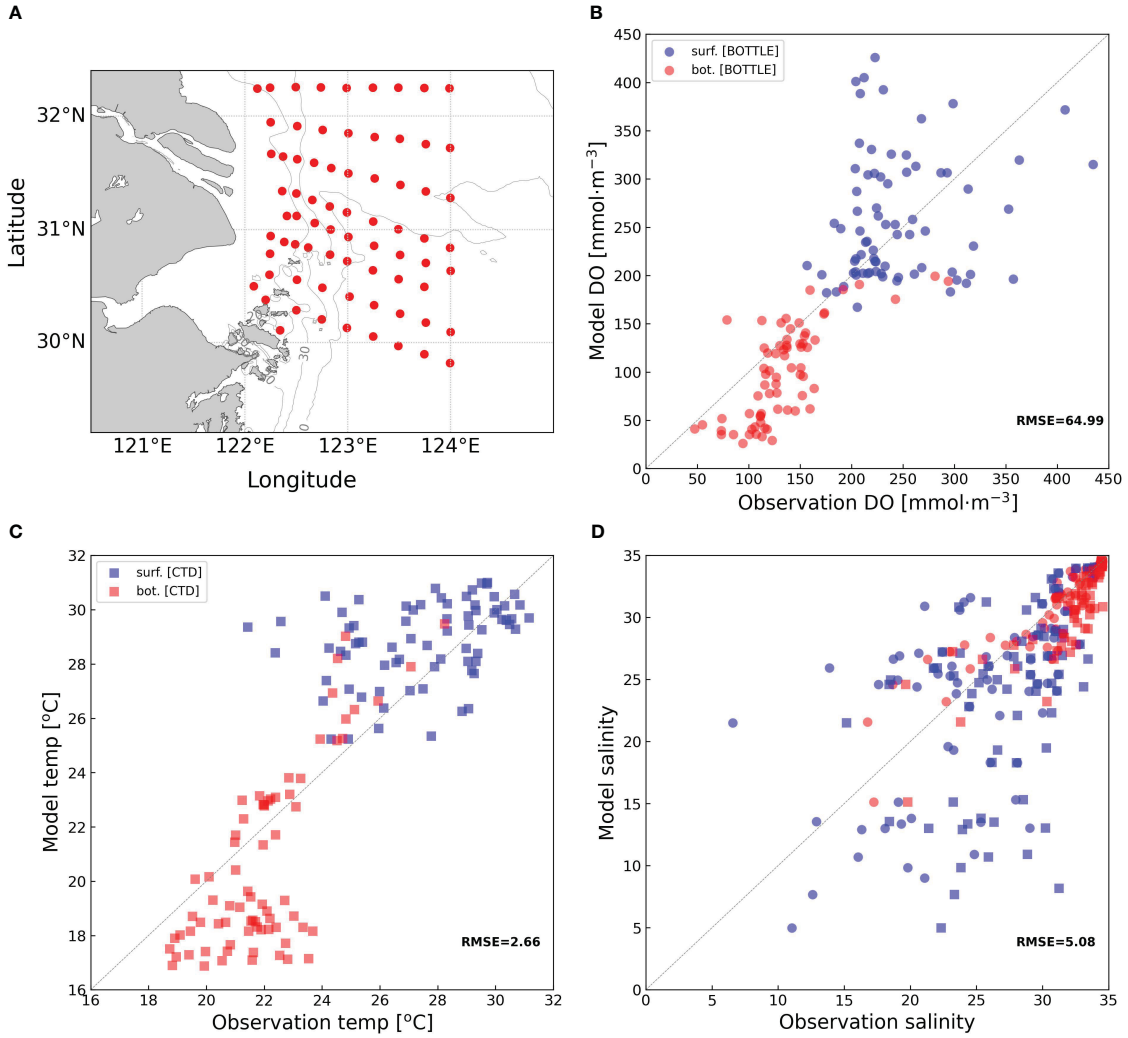

FIGURE 3
Model validation by *in-situ* observation in July 2017. The location of stations **(A)** and the validation results of dissolved oxygen **(B)**, temperature **(C)**, and salinity **(D)**. The blue and red circles represent surface and bottom data, respectively. The circle and square represent data collected by bottle and CTD, respectively.

and blue circles in Figure 4E). Then, the Changjiang diluted water shifted northeastward, while the surface low-salinity water along the Zhejiang Coast gradually retreated (Figures 4F-H). The surface salinity of site P2 increased to above 31, while that of site P1 remained below 31 under the continuous influence of the Changjiang diluted water. Thus, there was a redistribution process of the Changjiang diluted water during the four periods.

Surface chlorophyll between July 6-20 was checked to investigate the variations of surface primary production (represented by chlorophyll concentration) (Figures 4I-L). The high chlorophyll mainly distributed off the Changjiang estuary and along the Zhejiang Coast, while the high values north of 30°N were constrained within the range of the Changjiang diluted water (Figures 4I-L). The chlorophyll concentration and areal extent of high chlorophyll were larger off the Changjiang estuary (Figures 4I-L). The highest chlorophyll concentration off the Changjiang estuary on July 20 exceeded 12 mg·m^{-3}, while that along the Zhejiang Coast was approximately 7 mg·m^{-3} (Figures 4I-L). During the redistribution of Changjiang diluted water, the chlorophyll concentration off the estuary gradually increased, and the high chlorophyll area expanded northeast (Figures 4J-L). On the other hand, the moderate chlorophyll area (around 6 mg·m^{-3}) offshore of the Zhejiang Coast on July 6 disappeared (Figures 4I, L).

The vertical variation of chlorophyll in the whole water column was further explored by calculating the depth-integrated chlorophyll. The distribution of depth-integrated chlorophyll showed similarities to surface chlorophyll (Figures 4M-P). High depth-integrations (about 60-80 mg·m^{-2}) were found in an offshore area of the Zhejiang Coast (Figures 4L, P) with surface chlorophyll concentrations below 2 mg·m^{-3} (dark green isolines in Figures 4I-P). This area was outside the range of Changjiang diluted water, suggesting other nutrients sources supporting the phytoplankton growth. Comparisons between the spatial distribution of surface chlorophyll and depth-integrated chlorophyll, we found distinct vertical distribution of chlorophyll distribution between the Zhejiang Coast and the region off the Changjiang estuary, such

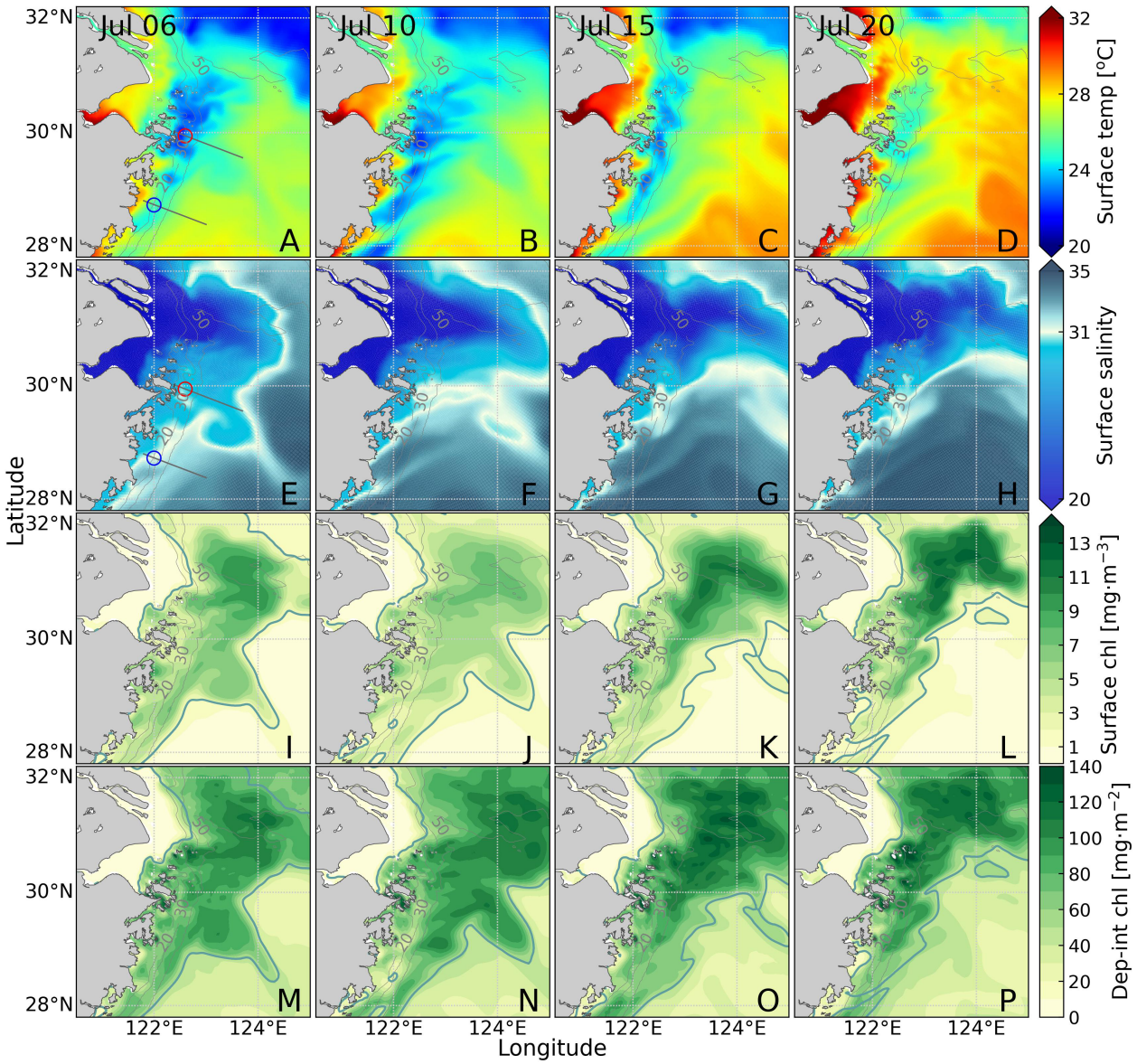

FIGURE 4
Sea surface temperature **(A-D)**, sea surface salinity **(E-H)**, sea surface chlorophyll **(I-L)**, and depth-integrated chlorophyll **(M-P)** for the four periods. In panels **(A, E)**, the grey lines indicate the locations of sections S1 and S2, and the red and blue hollow circles are the locations of sites P1 and P2. In panels **(E-H)**, the white lines indicate the 31 isohalines. In panels **(I-P)**, the dark green lines indicate the 2 mg·m^{-3} chlorophyll contour.

that subsurface chlorophyll maximum existed in the offshore region of Zhejiang Coast.

3.2 Hypoxia characteristics

The hypoxia threshold was often defined as 62.5 mmol·m^{-3} (Rabouille et al., 2008; Zhu et al., 2011; Zhang et al., 2021), and this study used 60 as the threshold for hypoxia for simplicity. Different dissolved oxygen concentration thresholds of 20, 40, 60, and 80 mmol·m^{-3} (with an interval of 20) were used to comprehensively investigate the degree of oxygen depletion (severe, moderate, usual, mild hypoxia). The frequency of hypoxia with different thresholds during the summer months (June, July, and August) was obtained by accumulating the time of hypoxia occurrences (Figure 5). The model results show that a small area (around 92 km^2) off the Changjiang estuary experienced severe hypoxia (20 mmol·m^{-3}) (Figure 5A). The frequency of hypoxia occurrence gradually increased with the threshold for dissolved oxygen. Both the regions off the Changjiang estuary and along the Zhejiang Coast had larger areas of hypoxia (60 mmol·m^{-3}) compared to moderate hypoxia (40 mmol·m^{-3}) (Figures 5B, C). The extent of moderate hypoxia off the Changjiang estuary was 1388 km^2, and 313 km^2 along the Zhejiang Coast. However, the extent of hypoxia off the Changjiang estuary increased to 5725 km^2, and also expanded to 1427 km^2 along the Zhejiang Coast. With a threshold of 80 mmol·m^{-3}, the extent of mild hypoxia almost doubled and increased to 11741 km^2 and 3054 km^2 off the Changjiang estuary

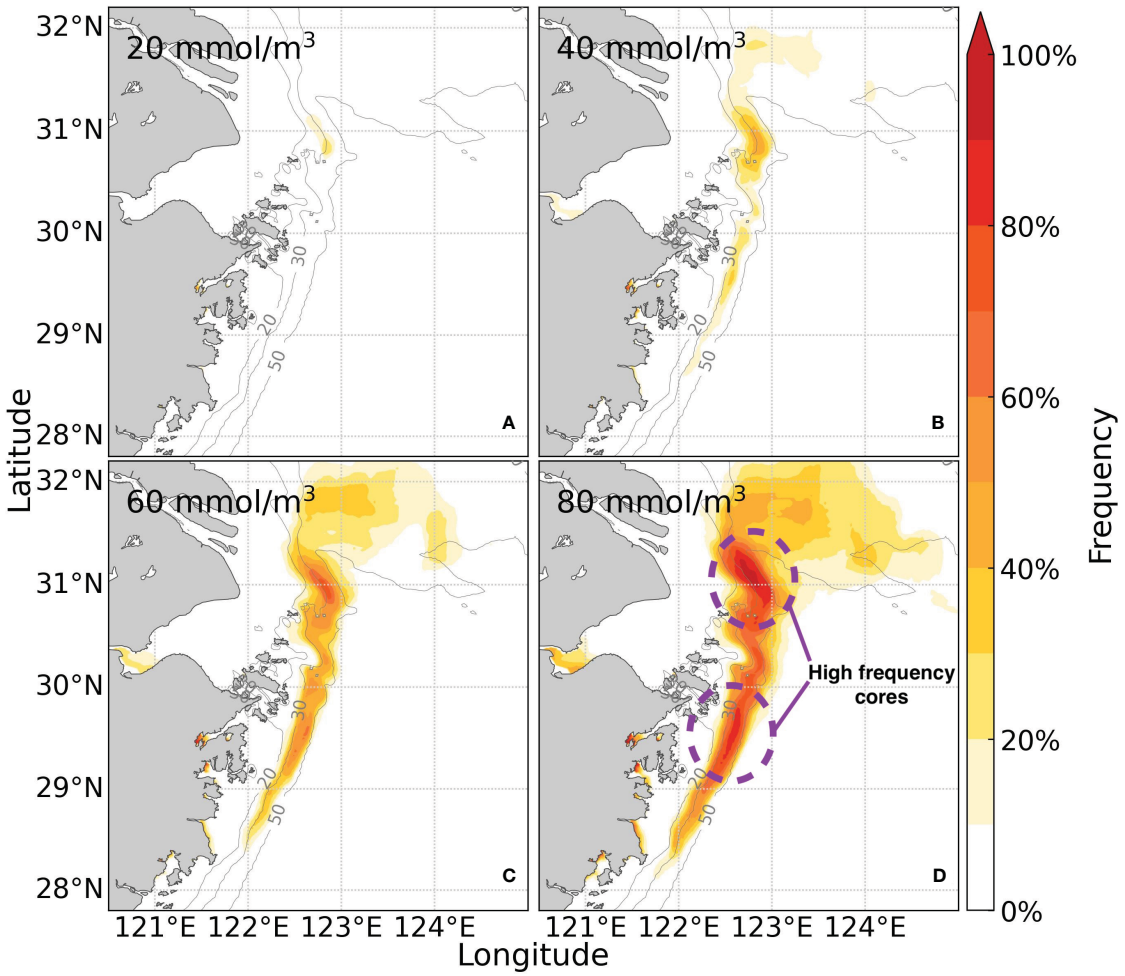

FIGURE 5
The frequency of hypoxia events with different thresholds at the bottom of the study area in summer 2017.

and along the Zhejiang Coast, respectively (Figure 5D). Mild hypoxia off the Changjiang estuary expanded beyond 32°N and 124°E (Figure 5D). Although the areal expansion off the Zhejiang Coast showed trivial changes, the occurrence frequency increased significantly (Figure 5D). Overall, hypoxia events along the Zhejiang Coast primarily occurred between the 20-50 m isobaths.

There were two distinct high-frequency regions of hypoxia: the northern core near the submarine canyon and the southern core at approximately 29.5°N along the Zhejiang Coast (Figure 5D). The frequency of hypoxia was low off the Changjiang estuary in average, despite its large coverage compared to that along the Zhejiang Coast. Outside the northern core, the occurrence frequency ranged from 10% to 20% at a threshold of 40 mmol·m^{-3}, while inside the core, it ranged from 30% to 40% (Figure 5B). The core region exhibited even higher frequency ranges of 60-70% and 80-90% with higher dissolved oxygen thresholds, but areas outside the core region remained below 50% (Figures 5C, D). Along the Zhejiang Coast, the frequency differences between the core and outside-core regions were relatively small. At thresholds of 40, 60, and 80 mmol·m^{-3}, the frequency of hypoxia outside the southern core region spanned from 10% to 60%, while inside the core region, it spanned from 20% to 80% (Figures 5B-D). Mild hypoxia was generally more frequent and longer-lasting along the Zhejiang Coast compared to that off the Changjiang estuary. Therefore, to analyze the processes of oxygen depletion along the Zhejiang Coast, we examined the variables along two transects (S1, located in the northern part of Zhejiang Coast; S2, located in the middle part of Zhejiang Coast, as shown in Figure 1B) and their corresponding nearshore sites (Figure 1B).

3.3 The sectional view of Zhejiang Coast

3.3.1 Section S1

Section S1, located at the intersection of Changjiang estuary and Zhejiang Coast (Figure 1B), experienced the presence of low-salinity water (blue contours in Figures 6A-H) covering the upper layer from July 6 to July 20. The nitrate concentration in the nearshore area (inner end of the section) surpassed 16 mmol·m^{-3} and reduced seaward (Figures 6A-D). The expansion of low-salinity water with high-nitrate in the upper layer gradually contracted during the redistribution of the Changjiang diluted water. By July 15 and 20,

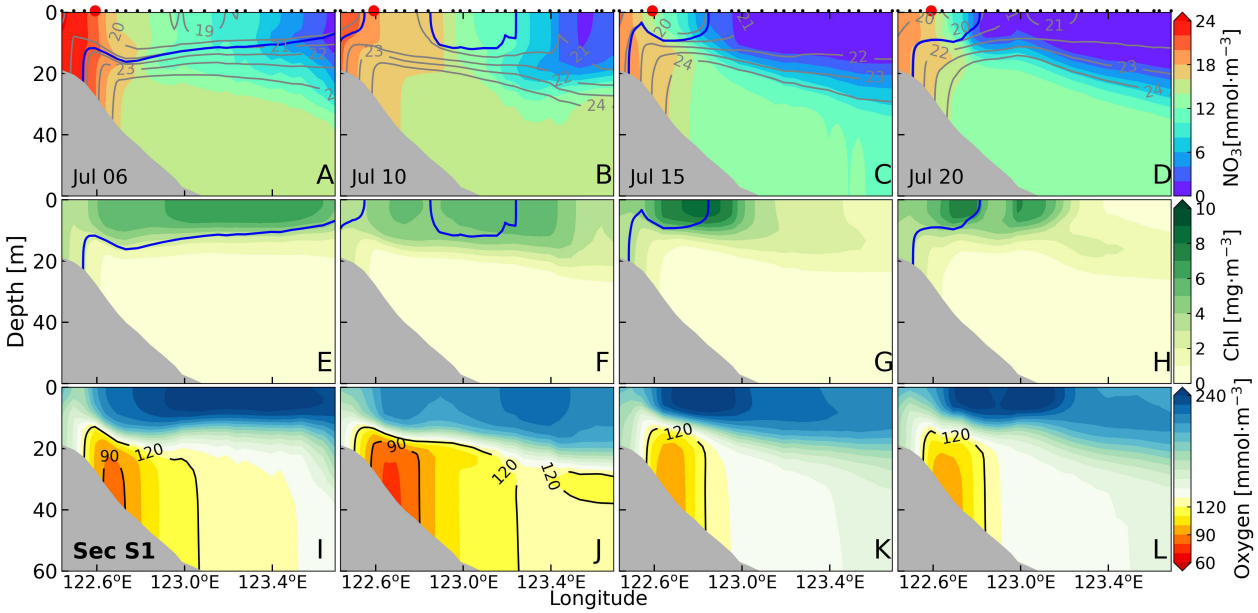

FIGURE 6
Sectional distributions of nitrate **(A-D)**, chlorophyll **(E-H)**, and dissolved oxygen **(I-L)** for section S1 for four periods. The grey lines, red and black dots in panels **(A-D)** are the isopycnals, the locations of site P1, and model grids, respectively. The blue lines in panels **(A-H)** are the 31 isohalines. The black lines in panels **(I-L)** represent the 90 and 120 mmol·m^{-3} isooxylines.

Changjiang diluted water was generally constrained to the nearshore region, the extremely low nitrate was seen in the offshore area (outer end of the section) (Figures 6C, D). In addition, the presence of low-salinity water impacted the vertical density structure. With the retreat of the surface low-salinity water, the offshore surface-bottom density difference decreased from larger than 4 kg·m^{-3} to about 3 kg·m^{-3} (Figures 6C, D).

The chlorophyll concentration in the range of low-salinity water was relatively high (Figures 6E-H). The chlorophyll distribution was similar to the low-salinity water. As the low-salinity water contracted shoreward between July 15 and 20, the surface chlorophyll concentration in the nearshore area maintained exceeding 7 mg·m^{-3}, while that in the offshore area decreased to a very low level (Figures 6G, H). The areas with high dissolved oxygen concentration in the upper layer were generally co-located with those high chlorophyll concentration in the upper layer (Figures 6I-L). The minimum dissolved oxygen concentration was below 100 mmol·m^{-3} throughout all four periods. To distinguish the different degrees of oxygen depletion, we referred to the hypoxic and low-oxygen water with thresholds of 60 mmol·m^{-3} (equivalent to around 2 mg/L) and 90 mmol·m^{-3} (around 3 mg/L), respectively. On July 6 and 10, low-oxygen water existed along the nearshore slope, with dissolved oxygen concentration below 90 mmol·m^{-3} (Figures 6I, J). Meanwhile, the bottom dissolved oxygen concentration of the offshore area was beyond 120 mmol·m^{-3}. The nearshore low-oxygen water disappeared during the redistribution of Changjiang diluted water, and the offshore dissolved oxygen concentration increased to above 140 mmol·m^{-3} (Figures 6K, L).

To further investigate the nearshore oxygen depletion, we chose site P1 on section S1 and examined the variable variations over time (Figure 7). For the majority of July, the upper layer of site P1 experienced low-salinity water (Figure 7A). The nutrient concentration in the upper layer was relatively sufficient, with nitrate concentration mostly larger than 12 mmol·m^{-3} (Figure 7B). The chlorophyll concentration of the upper layer was consistently high, mostly larger than 4 mg·m^{-3} (Figure 7D). On July 20, a large amount of low-salinity water reached site P1, causing a sharp decrease in salinity (Figure 7A), and a subsequent increase in surface chlorophyll concentration (Figure 7D). After that, the surface nitrate concentration decreased significantly (lower than 12 mmol·m^{-3}) (Figure 7B). There was an upwelling event on July 10, indicated by the low-temperature, high-salinity, and high-density water (19°C, 33 psu, 1023 kg·m^{-3}) from the bottom to a depth of approximately 15 m (Figures 7A, C, E). The presence of other upwelling events was also found on July 2 and 17. However, the increase in chlorophyll associated with upwelling was difficult to identify due to the intense impacts from the Changjiang diluted water (Figures 7B, D).

The bottom dissolved oxygen concentration at site P1 was typically below 120 mmol·m^{-3} (Figure 7F). On July 4, there was a sharp increase in the bottom dissolved oxygen concentration, coinciding with a decreased density difference (Figures 7F, 8A). Despite a density difference above 2 kg·m^{-3} and a surface chlorophyll concentration higher than 5 mg·m^{-3} from July 10 to 20, the bottom dissolved oxygen concentration was relatively high (over 90 mmol·m^{-3}). The Changjiang diluted water shifted direction after July 10 (Figures 4E-H), and there was a highly dynamic environment during this time. According to Zhou et al. (2020), this dynamic environment can lead to the spatial separation of areas with high chlorophyll and locations with oxygen depletion. Thus,

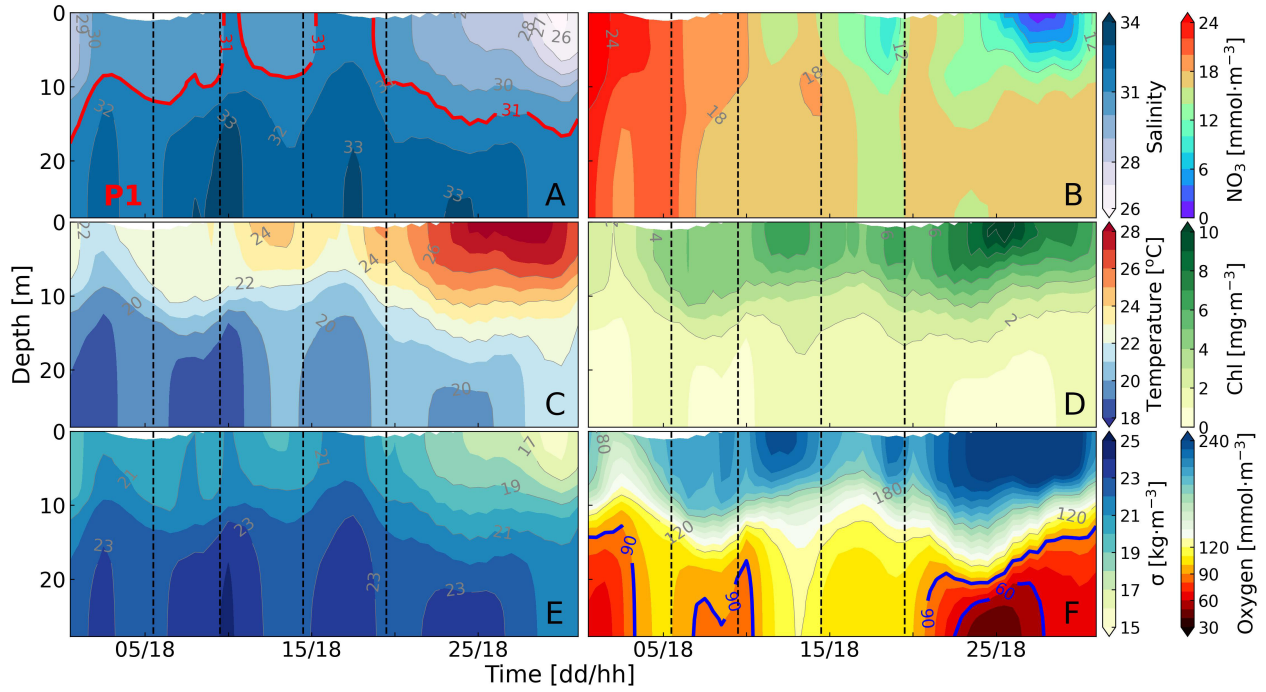

FIGURE 7
Time series profiles of salinity **(A)**, nitrate **(B)**, temperature **(C)**, chlorophyll **(D)**, density anomaly **(E)**, and dissolved oxygen **(F)** profiles at site P1 in July. The red lines in panel A are the 31 isohalines. The blue lines in panel **(F)** represent the 60 and 90 mmol·m^{-3} isooxylines. The time format is "day/hour [dd/hh]".

the mild oxygen depletion between July 10 and 20 may be attributed to the lateral delivery of high-oxygen water. After July 20, a substantial volume of low-salinity water arrived, causing a rapid increase in surface-bottom density differences, reaching 6 kg·m^{-3} (Figure 8A). It led to rapid development of low-oxygen condition and hypoxia from July 25 onward (Figure 7F). Overall, the depths of pycnocline and oxycline at site P1 exhibited similar variations in July (Figure 8B).

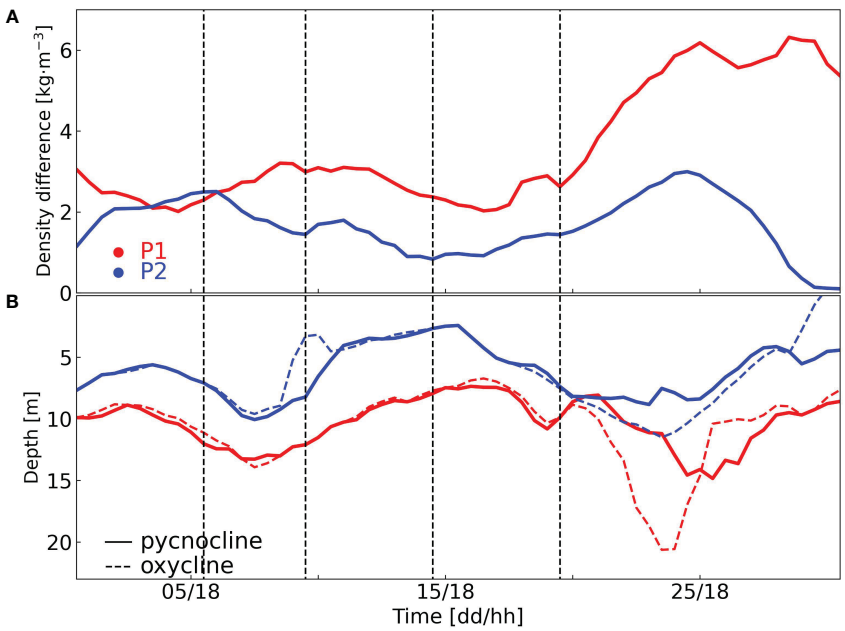

FIGURE 8
Time series of density difference **(A)**, the depths of pycnocline and oxycline **(B)** at sites P1 and P2 in July. The red and blue lines represent sites P1 and P2, respectively. The solid and dashed lines in panel **(B)** represent the depths of pycnocline and oxycline, respectively. The time format is "day/hour [dd/hh]".

3.3.2 Section S2

Section S2 is located farther from the Changjiang estuary than section S1 (Figure 1B). The 31 isohaline only appeared before July 6 (Figures 9A, E), and section S2 was free from the impacts of Changjiang diluted water after July 6. Consequently, the nitrate concentration exhibited a typical bottom-up vertical distribution with the highest values at the bottom (Figures 9A-D). The high nitrate concentration at the nearshore surface decreased from greater than 8 mmol·m^{-3} on July 6 to a very low level by July 20 (Figures 9A-C). The offshore nitrate was genuinely deficient at the surface. High-nitrate (over 10 mmol·m^{-3}) and high-density (greater than 1024 kg·m^{-3}) water tongue was seen along the slope. The density difference of the nearshore area on July 6 was greater than 4 kg·m^{-3} and subsequently decreased to approximately 2 kg·m^{-3}, leading to sparser distribution of isopycnals.

During all four periods, the chlorophyll concentration along section S2 was consistently lower than that along section S1 (Figures 9E-H). On July 6, the nearshore chlorophyll concentration in the upper layer exceeded 6 mg·m^{-3} (Figure 9E) and dissolved oxygen concentration was low (Figure 9I). Under the deficient nutrients condition in the upper layer, phytoplankton growth was restricted and phytoplankton bloomed in the subsurface layer (Figures 9F-H). On July 20, the surface chlorophyll concentration decreased to about 2 mg·m^{-3}, with the highest chlorophyll concentrations occupied the depth of about 10 m (Figure 9H). The subsurface chlorophyll maximum occurred immediately underneath the main pycnocline. The minimum dissolved oxygen concentration was greater than 110 mmol·m^{-3} after July 6 (Figures 9I-L).

We chose a nearshore site P2 on section S2 for a further investigation in oxygen depletion. The surface salinity at site P2 remained consistently high after July 6 (Figure 10A). The nitrate concentration in the upper layer gradually decreased after July 6, reaching an extremely low level (Figure 10B). The redistribution of Changjiang diluted water weakened its southern branch (Figures 4E-H). As a result, the riverine influences at site P2 retreated soon after July 6 (Figure 10A). In comparison to site P1, the chlorophyll concentration at site P2 was generally lower (Figure 10D). As the upper layer underwent nutrients declined, the chlorophyll concentration decreased from approximately 5 mg·m^{-3} on July 5 to less than 2 mg·m^{-3} after July 22 (Figure 10B). Meanwhile, phytoplankton growth occurred in the subsurface layer (Figure 10D). An upwelling event took place on July 10, characterized by the uplift of low-temperature, high-salinity, high-density, and nutrient-rich water (21°C, 34 psu, 1024 kg·m^{-3}, and 6-8 mmol·m^{-3}) to a depth of approximately 10 m (Figures 10A, C, E). The nutrients associated with this upwelling (approximately 8 mmol·m^{-3}) resulted in a surface chlorophyll concentration increase to 4 mg·m^{-3} (Figures 10B, D). The chlorophyll concentration peaked at the subsurface layer while the surface nutrients were deficient (Figure 10D).

The bottom dissolved oxygen concentration was higher than 120 mmol·m^{-3}, except for two low-oxygen periods on July 5 and 25 (Figure 10F). These two low-oxygen events occurred simultaneously with density differences exceeding 2 kg·m^{-3} (Figure 8A). Between July 10 and 20, the bottom oxygen concentration maintained above 120 mmol·m^{-3} (Figure 10F). Although the chlorophyll concentration remained mostly greater than 4 mg·m^{-3} during this period, the density difference is smaller than 2 kg·m^{-3} (Figures 8A, 10D). The density difference gradually increased after July 20 due to the warmer upper layer, but remained lower than the density difference at site P1 (Figures 8A, 10C). On July 25, a low-oxygen event occurred at the bottom of site P2, coinciding with the same period as site P1. However, site P2 did not

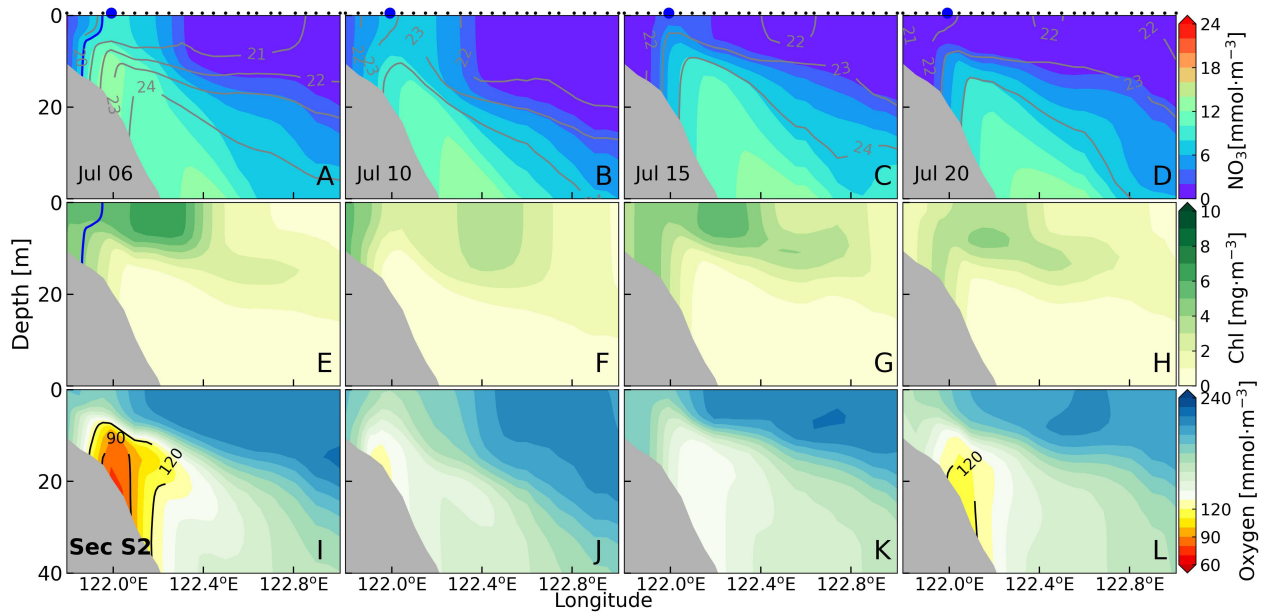

FIGURE 9
Sectional distributions of nitrate **(A-D)**, chlorophyll **(E-H)** and dissolved oxygen **(I-L)** in section S2 for four periods.

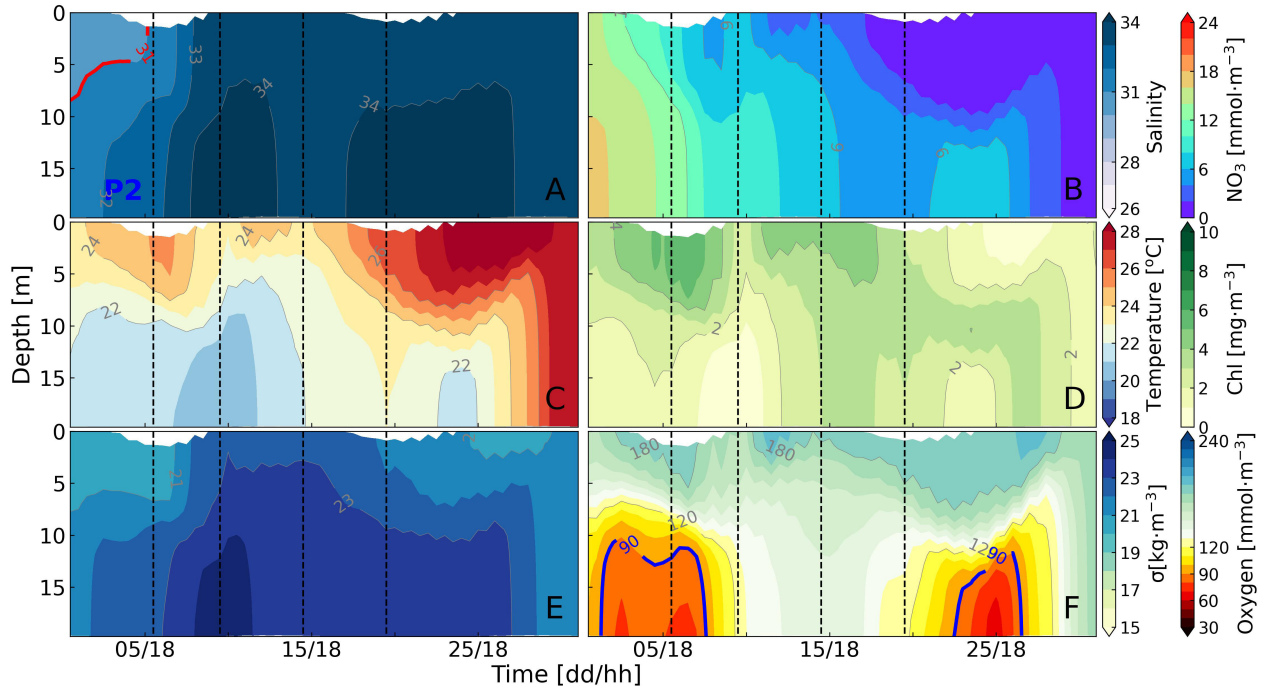

FIGURE 10
Time series profiles of salinity **(A)**, nitrate **(B)**, temperature **(C)**, chlorophyll **(D)**, density anomaly **(E)**, and dissolved oxygen **(F)** profiles at site P2 in July.

experience hypoxia like site P1 did, and bottom oxygen concentration at P2 was generally higher than that at P1 (Figures 7F, 10F). Same as site P1, the pycnocline and oxycline depth at site P2 also exhibited similar variations over time (Figure 8B).

4 Discussion

4.1 The impact of upwelling

Upwelling, characterized by low temperature in surface, is commonly observed on the Zhejiang Coast (Hu and Wang, 2016; Chi et al., 2020; Wei et al., 2021). Upwelling-favorable wind can induce near-coast upwelling and support phytoplankton growth (Luo et al., 2023). In this study, the upwelling associated with the distortion of isopycnal caused by the confluence of Changjiang diluted water, shelf water, and Kuroshio subsurface water was the focus. The formation of upwelling depends on density gradient and diapycnal transport (Zhu, 2003; Lü et al., 2006; Lü et al., 2007; Zhang et al., 2015). To identify the location of bottom salinity fronts and determine their probability of occurrence during summer, we followed Wu and Wu (2018) and employed the gradient method (Huang et al., 2010; He et al., 2016) (Figure 11). The high-frequency bottom salinity fronts predominantly emerged between the 20-50 m isobaths along the Zhejiang Coast, which was co-located with the hotspot of hypoxia (Figure 5). The Zhejiang Coast was influenced by the confluence of Changjiang diluted water, shelf water, and Kuroshio subsurface water. The meeting of water masses with distinct density resulted in concentrated isopycnals (frontogenesis), and the distortion of density surface caused diapycnal transport (convergence), and the convergent flow occurred at the foot of the front and upwelled along the front (Zhang et al., 2015). The water masses with distinct density influenced site P1 for longer time than site P2 in July (Figure 7A, 10A). Although sites P1 and P2 were both situated near the vicinity of the salinity fronts, the front occurrence frequency at P2 was much lower (Figure 11) and the impacts of upwelling at site P1 were more intense than at site P2 (Figure 4A-D). It indicates that the meet of Changjiang diluted water and Kuroshio subsurface water would intensify upwelling, leading to more intense impacts of Kuroshio intrusion. The uplifted subsurface/bottom materials along tilted isopycnals reached the upper layer and offshore area to supply extra nutrients (Chen et al., 2021), supporting the growth of phytoplankton in this region and leading to the further decomposition of organic matter and oxygen depletion (Feng et al., 2014; Wei et al., 2021; Lao et al., 2023a).

Upwelling-induced phytoplankton blooms can lead to increased organic matter production and subsequent oxygen depletion in the water column (Bianucci et al., 2011). Similar findings have been reported in other upwelling systems. For example, upwelling on the New Jersey shelf resulted in a significant increase in particulate organic carbon and a 75% depletion of oxygen in the bottom water (Glenn et al., 2004). In the California Current System, the heterogeneous alongshore pattern of nearshore oxygen can be explained by the interplay between variability in local upwelling intensity and subsequent primary production (Cheresh and Fiechter, 2020). The findings in this study are consistent with previous studies (Chen et al., 2004; Chen et al., 2021). Furthermore, this study found that upwelling

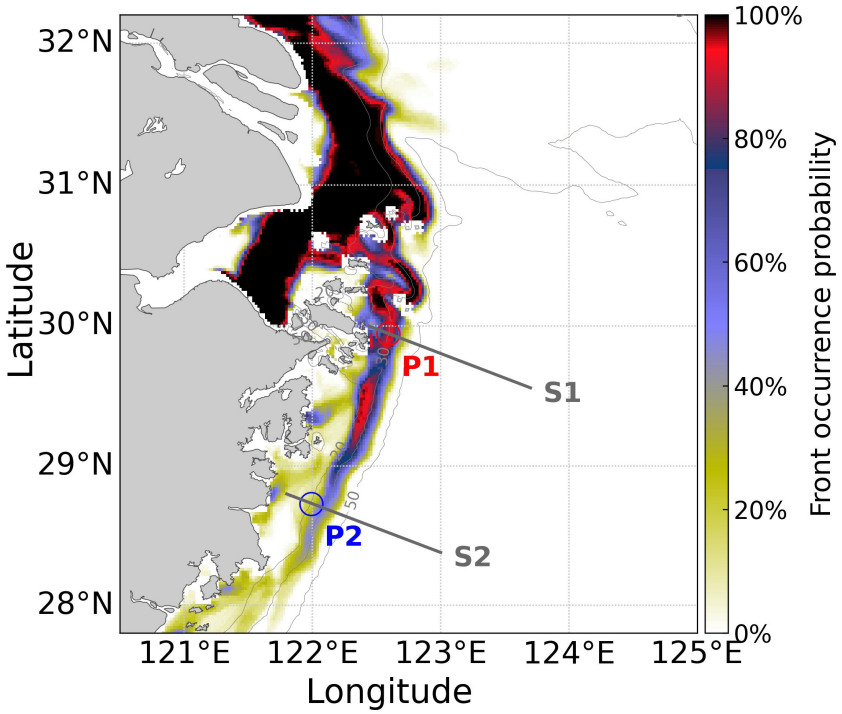

FIGURE 11
The occurrence probability of bottom salinity fronts in summer 2017. The gray lines indicate the locations of sections S1 and S2. The red and blue hollow circles indicate the locations of sites P1 and P2, respectively.

also temporally relieved nutrients deficiency at the subsurface of offshore area along the Zhejiang Coast, resulting in decent depth-integrated chlorophyll (Figure 10D). This indicated that the oceanic nutrients were further transported offshore along isopycnals and reached the offshore euphotic zone.

4.2 The different effects of Changjiang and Kuroshio on oxygen depletion

The isopycnals concentrated surrounding the oxygen deficiency water (Figures 6I-L), and the depth of the pycnocline and oxycline exhibited similar variations over time at both sites (Figure 8B). This indicates that stratification is necessary for the sustainment of oxygen depletion by limiting vertical oxygen exchange. Thus, the low-salinity water delivered from Changjiang can significantly enhance the strength of stratification, which limits the vertical exchange of oxygen and facilitates the formation of hypoxia (Zhou et al., 2017; Zhang et al., 2021). Kuroshio also contributes to the formation of hypoxia (Zhou et al., 2018). Model results show that there was a high depth-integration chlorophyll (about 60-80 $mg{\cdot}m^{-2}$) but low surface chlorophyll (below 2 $mg{\cdot}m^{-3}$) offshore area along the Zhejiang Coast (Figures 4L, P). This area was outside the range of Changjiang diluted water, implying nutrients from Kuroshio supporting the phytoplankton growth. Therefore, the Zhejiang Coast is influenced by both the southward branch of Changjiang diluted water and the intrusion of Kuroshio. The complex dynamic environment and various nutrients sources contribute to the spatially different oxygen depletion on the Zhejiang Coast (P1, P2, S2, and S2). Hypoxia events along the Zhejiang Coast are always confined near the coast, which was different from that off the Changjiang estuary (Figure 5). Water in regions deeper than 50 m rapidly exchanges with water from Kuroshio, the dissolved oxygen concentration in which is typically higher than that in the high-primary-production coastal water. The consumed oxygen can be rapidly replenished *via* lateral advection. On the other hand, the concentrated isobath along the Zhejiang Coast acts as a natural barrier to prevent direct water mass exchanges. The Mid Atlantic Bight is a typical prototype that has similar geographical features that trigger similar physical and biogeochemical processes (Zhang and Gawarkiewicz, 2015; Zhang et al., 2023). Although Changjiang diluted water occasionally appeared and impacted site P2, Kuroshio subsurface water was the main factor regarding physical processes and biogeochemical cycles (Figures 7F, 10F).

Changjiang and Kuroshio subsurface water jointly regulate the formation and sustainment of low oxygen condition over the continental shelf. However, Changjiang and Kuroshio play spatially distinct roles in the phytoplankton growth (Xu et al., 2020) and vertical stratification (Figure 8A), and subsequently the dissolved oxygen depletion over the shelf (Große et al., 2020). The distribution of chlorophyll off the Changjiang estuary differed from that south of 30°N (Figures 4I-L). The region off the Changjiang estuary exhibited large areal expansion of high surface chlorophyll, generally constrained within the range of Changjiang diluted water. During the co-existence of Changjiang diluted water and upwelled Kuroshio subsurface water, Changjiang is the controlling factor regarding the rapid development of high vertical stratification and

bottom hypoxia, such as site P1 and section S1. On the other hand, upwelled nutrients associated with Kuroshio subsurface water become the predominant fertilizer for phytoplankton growth along the Zhejiang Coast, such as site P2 and section S2. The vertical stratification associated with upwelling of Kuroshio subsurface water was mild due to the lack of the buoyant layer atop. The surface chlorophyll concentration and depth-integrated chlorophyll along the concentrated isobath on the Zhejiang Coast were relatively lower. However, the offshore high depth-integrated chlorophyll indicated the existence of subsurface chlorophyll maximum (Figures 4P, 9H, 10D). Phytoplankton growth at a depth of the nitracline is one of the reasons for the subsurface chlorophyll maximum formation (Barbieux et al., 2019). The findings suggest that nutrients from Kuroshio were also important for the growth of subsurface phytoplankton in offshore areas on the Zhejiang Coast.

The delivery of nutrient-rich water masses can stimulate phytoplankton growth (Lao et al., 2022 and Oziel et al., 2017; Lao et al., 2023b). This promoted phytoplankton growth leads to a rise in organic matter. The decomposition of organic matter significantly consumes dissolved oxygen, ultimately resulting in the formation of hypoxia (Chen et al., 2021; Wei et al., 2021; Sun et al., 2022; Sathish et al., 2023). In the case of Changjiang, the substantial nutrients in the upper layer greatly stimulated phytoplankton growth (Figures 8A, B). Additionally, the freshwater strengthened vertical stratification by enlarging the density difference from bottom to surface. The intense degradation of organic matter at the subsurface layer, coupled with simultaneous strong vertical stratification, leading to rapid oxygen depletion and the development of bottom hypoxia. However, the hypoxia events off the Changjiang estuary were typically transient (short sustainment in time) (Figure 5) due to the mobile Changjiang diluted water (Zhang et al., 2018). On the other hand, Kuroshio subsurface water intrusion was the strongest during summer (Yang et al., 2018), persistently delivering oceanic nutrients *via* upwelling. The oceanic nutrients also fertilized phytoplankton growth. Although the stratification strength was not significantly intensified, the increased organic matter associated with phytoplankton continuously consumed dissolved oxygen. The frequency of severe hypoxia along the Zhejiang Coast was lower overall while that of mild hypoxia was more prolonged (Figure 5). It has been observed that the nutrients from Kuroshio Intermediate Water, a significant source of coastal upwelling water, have increased as a result of weakened ventilation in the North Pacific Intermediate Water (Lui et al., 2014). Zhou et al. (2017) suggested that a Kuroshio nutrient increase can cause the maximum hypoxia extent in August to increase by 32%. This indicates that the oxygen depletion along the Zhejiang Coast would be intensified by the potentially elevated nutrient delivery from Kuroshio in the future.

The dissolved oxygen concentration of Kuroshio subsurface water, 125 mmol·m^{-3} (Wang et al., 2023), also has far-reaching impacts on the continental shelf oxygen dynamics. The Kuroshio subsurface water preconditions the shelf with relatively low dissolved oxygen prior to the approaching of hypoxic season, and replenishes the hypoxic zone as an oxygen source during hypoxic season (Chi et al., 2020). Deoxygenation is happening and accelerating globally with oxygen loss rate spanning a wide range in different latitudes or regions (Ito et al., 2017; Oschlies et al., 2018). Hence, deoxygenation of Kuroshio would further intensify its influence on the oxygen dynamics over the continental shelf, especially along the Zhejiang Coast, with high confidence in the future.

5 Conclusions

A coupled physical-biogeochemical model was used to investigate the contributions of Changjiang and Kuroshio to oxygen depletion over the continental shelf over the East China Sea. The regions off the Changjiang estuary and along the Zhejiang Coast have distinct oxygen depletion features. Changes in nutrients, chlorophyll, stratification, and oxygen were linked with the delivery of Changjiang diluted water and Kuroshio subsurface water. Changjiang diluted water spread southward and occasionally influenced Zhejiang coastal region, especially near Zhoushan. Its influences along the Zhejiang Coast weakened southward, letting the effects of upwelling of Kuroshio subsurface water stand out. The persistent intrusion of Kuroshio subsurface water continuously fertilized phytoplankton growth, resulting in mild oxygen depletion and sustained prolonged low-oxygen condition. Upwelling emerged as a key mechanism by which nutrients from Kuroshio affected the inner shelf along the Zhejiang Coast. Additionally, this study indicated that upwelling of Kuroshio subsurface water also caused phytoplankton growth at the subsurface of offshore areas.

Data availability statement

The original contributions presented in the study are included in the article/supplementary material. Further inquiries can be directed to the corresponding author.

Author contributions

HW: Investigation, Visualization, Writing – original draft, Writing – review & editing. WY: Writing – original draft. WZ: Supervision, Writing – original draft, Writing – review & editing. XZ: Writing – review & editing.

Funding

The author(s) declare financial support was received for the research, authorship, and/or publication of this article. This work was jointly supported by the Science and Technology Committee of Shanghai Municipal (No. 21JC1402500), the National Natural Science Foundation of China (No. 41876026), the open fund of Key Laboratory of Ocean Space Resource Management Technology, MNR (KF-2023-113), the National Programme on Global Change

and Air–Sea Interaction Phase II, Zhejiang Provincial Ten Thousand Talents Program (No. 2020R52038).

Conflict of interest

The authors declare that the research was conducted in the absence of any commercial or financial relationships that could be construed as a potential conflict of interest.

Publisher's note

References

Barbieux, M., Uitz, J., Gentili, B., de Fommervault, O. P., Mignot, A., Poteau, A., et al. (2019). Bio-optical characterization of subsurface chlorophyll maxima in the Mediterranean Sea from a Biogeochemical-Argo float database. *Biogeosciences* 16 (6), 1321–1342. doi: 10.5194/bg-16-1321-2019

Bianucci, L., Denman, K. L., and Ianson, D. (2011). Low oxygen and high inorganic carbon on the Vancouver Island Shelf. *J. Geophys. Research-Oceans* 116, 20. doi: 10.1029/2010jc006720

Breitburg, D., Levin, L. A., Oschlies, A., Gregoire, M., Chavez, F. P., Conley, D. J., et al. (2018). Declining oxygen in the global ocean and coastal waters. *Science* 359 (6371), 46. doi: 10.1126/science.aam7240

Chang, P. H., and Isobe, A. (2003). A numerical study on the Changjiang diluted water in the Yellow and East China Seas. *J. Geophys. Research-Oceans* 108 (C9), 1–17. doi: 10.1029/2002jc001749

Chen, C. T. A. (1996). The Kuroshio intermediate water is the major source of nutrients on the East China Sea continental shelf. *Oceanol. Acta* 19 (5), 523–527.

Chen, C. T. A. (2009). Chemical and physical fronts in the Bohai, Yellow and East China seas. *J. Mar. Syst.* 78 (3), 394–410. doi: 10.1016/j.jmarsys.2008.11.016

Chen, Y. L. L., Chen, H. Y., Gong, G. C., Lin, Y. H., Jan, S., and Takahashi, M. (2004). Phytoplankton production during a summer coastal upwelling in the East China Sea. *Continental Shelf Res.* 24 (12), 1321–1338. doi: 10.1016/j.csr.2004.04.002

Chen, C. C., Gong, G. C., and Shiah, F. K. (2007). Hypoxia in the East China Sea: One of the largest coastal low-oxygen areas in the world. *Mar. Environ. Res.* 64 (4), 399–408. doi: 10.1016/j.marenvres.2007.01.007

Chen, C. C., Shiah, F. K., Gong, G. C., and Chen, T. Y. (2021). Impact of upwelling on phytoplankton blooms and hypoxia along the Chinese coast in the East China Sea. *Mar. pollut. Bull.* 167, 9. doi: 10.1016/j.marpolbul.2021.112288

Chen, C. T. A., and Wang, S. L. (1999). Carbon, alkalinity and nutrient budgets on the East China Sea continental shelf. *J. Geophys. Research-Oceans* 104 (C9), 20675–20686. doi: 10.1029/1999jc900055

Cheresh, J., and Fiechter, J. (2020). Physical and biogeochemical drivers of alongshore pH and oxygen variability in the california current system. *Geophys. Res. Lett.* 47 (19), 9. doi: 10.1029/2020gl089553

Chi, L. B., Song, X. X., Yuan, Y. Q., Wang, W. T., Cao, X. H., Wu, Z. X., et al. (2020). Main factors dominating the development, formation and dissipation of hypoxia off the Changjiang Estuary (CE) and its adjacent waters, China. *Environ. pollut.* 265, 14. doi: 10.1016/j.envpol.2020.115066

Diaz, R. J., and Rosenberg, R. (2008). Spreading dead zones and consequences for marine ecosystems. *Science* 321(5891), 926–929. doi: 10.1126/science.1156401

Egbert, G. D., and Erofeeva, S. Y. (2002). Efficient inverse Modeling of barotropic ocean tides. *J. Atmosph. Ocean. Technol.* 19 (2), 183–204. doi: 10.1175/1520-0426(2002)019<0183:Eimobo>2.0.Co;2

Fedorov, K. N. (1986). *Physical nature and structure of oceanic fronts* (Springer-Verlag).

Feng, Y., Fennel, K., Jackson, G. A., DiMarco, S. F., and Hetland, R. D. (2014). A model study of the response of hypoxia to upwelling-favorable wind on the northern Gulf of Mexico shelf. *J. Mar. Syst.* 131, 63–73. doi: 10.1016/j.jmarsys.2013.11.009

Feng, Y., Friedrichs, M. A. M., Wilkin, J., Tian, H. Q., Yang, Q. C., Hofmann, E. E., et al. (2015). Chesapeake Bay nitrogen fluxes derived from a land-estuarine ocean biogeochemical modeling system: Model description, evaluation, and nitrogen budgets. *J. Geophys. Research-Biogeosci.* 120 (8), 1666–1695. doi: 10.1002/2015jg002931

Fennel, K., Hu, J. T., Laurent, A., Marta-Almeida, M., and Hetland, R. (2013). Sensitivity of hypoxia predictions for the northern Gulf of Mexico to sediment oxygen consumption and model nesting. *J. Geophys. Research-Oceans* 118 (2), 990–1002. doi: 10.1002/jgrc.20077

Fennel, K., and Laurent, A. (2018). N and P as ultimate and proximate limiting nutrients in the northern Gulf of Mexico: implications for hypoxia reduction strategies. *Biogeosciences* 15 (10), 3121–3131. doi: 10.5194/bg-15-3121-2018

Fennel, K., Wilkin, J., Levin, J., Moisan, J., O'Reilly, J., and Haidvogel, D. (2006). Nitrogen cycling in the Middle Atlantic Bight: Results from a three-dimensional model and implications for the North Atlantic nitrogen budget. *Global Biogeochem. Cycles* 20 (3), 14. doi: 10.1029/2005gb002456

Glenn, S., Arnone, R., Bergmann, T., Bissett, W. P., Crowley, M., Cullen, J., et al. (2004). Biogeochemical impact of summertime coastal upwelling on the New Jersey Shelf. *J. Geophys. Research-Oceans* 109 (C12), 1–15. doi: 10.1029/2003jc002265

Gong, G. C., Chen, Y. L. L., and Liu, K. K. (1996). Chemical hydrography and chlorophyll a distribution in the East China Sea in summer: Implications in nutrient dynamics. *Continental Shelf Res.* 16 (12), 1561–1590. doi: 10.1016/0278-4343(96)00005-2

Große, F., Fennel, K., Zhang, H. Y., and Laurent, A. (2020). Quantifying the contributions of riverine vs. oceanic nitrogen to hypoxia in the East China Sea. *Biogeosciences* 17 (10), 2701–2714. doi: 10.5194/bg-17-2701-2020

He, S. Y., Huang, D. J., and Zeng, D. Y. (2016). Double SST fronts observed from MODIS data in the East China Sea off the Zhejiang-Fujian coast, China. *J. Mar. Syst.* 154, 93–102. doi: 10.1016/j.jmarsys.2015.02.009

Hu, J. Y., and Wang, X. H. (2016). Progress on upwelling studies in the China seas. *Rev. Geophys.* 54 (3), 653–673. doi: 10.1002/2015rg000505

Huang, D. J., Zhang, T., and Zhou, F. (2010). Sea-surface temperature fronts in the Yellow and East China Seas from TRMM microwave imager data. *Deep-Sea Res. Part Ii-Topical Stud. Oceanogr.* 57 (11-12), 1017–1024. doi: 10.1016/j.dsr2.2010.02.003

Isobe, A., Ando, M., Watanabe, T., Senjyu, T., Sugihara, S., and Manda, A. (2002). Freshwater and temperature transports through the Tsushima-Korea Straits. *J. Geophys. Research-Oceans* 107 (C7), 20. doi: 10.1029/2000jc000702

Ito, T., Minobe, S., Long, M. C., and Deutsch, C. (2017). Upper ocean O-2 trends: 1958-2015. *Geophys. Res. Lett.* 44 (9), 4214–4223. doi: 10.1002/2017gl073613

Jarvis, B. M., Greene, R. M., Wan, Y. S., Lehrter, J. C., Lowe, L. L., and Ko, D. S. (2021). Contiguous low oxygen waters between the continental shelf hypoxia zone and nearshore coastal waters of Louisiana, USA: interpreting 30 years of profiling data and three-dimensional ecosystem modeling. *Environ. Sci. Technol.* 55 (8), 4709–4719. doi: 10.1021/acs.est.0c05973

Lao, Q. B., Chen, F. J., Jin, G. Z., Lu, X., Chen, C. Q., Zhou, X., et al. (2023a). Characteristics and mechanisms of typhoon-induced decomposition of organic matter and its implication for climate change. *J. Geophys. Research-Biogeosci.* 128 (6), 18. doi: 10.1029/2023jg007518

Lao, Q. B., Liu, S. H., Ling, Z., Jin, G. Z., Chen, F. J., Chen, C. Q., et al. (2023b). External dynamic mechanisms controlling the periodic offshore blooms in Beibu gulf. *J. Geophys. Research-Oceans* 128 (6), 14. doi: 10.1029/2023jc019689

Lao, Q. B., Zhang, S. W., Li, Z. Y., Chen, F. J., Zhou, X., Jin, G. Z., et al. (2022). Quantification of the seasonal intrusion of water masses and their impact on nutrients in the Beibu gulf using dual water isotopes. *J. Geophys. Research-Oceans* 127 (7), 21. doi: 10.1029/2021jc018065

Laurent, A., Fennel, K., Cai, W. J., Huang, W. J., Barbero, L., and Wanninkhof, R. (2017). Eutrophication-induced acidification of coastal waters in the northern Gulf of Mexico: Insights into origin and processes from a coupled physical-biogeochemical model. *Geophys. Res. Lett.* 44 (2), 946–956. doi: 10.1002/2016gl071881

Levin, L. A., Ekau, W., Gooday, A. J., Jorissen, F., Middelburg, J. J., Naqvi, S. W. A., et al. (2009). Effects of natural and human-induced hypoxia on coastal benthos. *Biogeosciences* 6 (10), 2063–2098. doi: 10.5194/bg-6-2063-2009

Liblik, T., Wu, Y. J., Fan, D. D., and Shang, D. H. (2020). Wind-driven stratification patterns and dissolved oxygen depletion off the Changjiang (Yangtze) Estuary. *Biogeosciences* 17 (10), 2875–2895. doi: 10.5194/bg-17-2875-2020

Lie, H. J., Cho, C. H., Lee, J. H., and Lee, S. (2003). Structure and eastward extension of the Changjiang River plume in the East China Sea. *J. Geophys. Research-Oceans* 108 (C3), 14. doi: 10.1029/2001jc001194

Liu, Z. Q., Gan, J. P., Wu, H., Hu, J. Y., Cai, Z. Y., and Deng, Y. F. (2021). Advances on coastal and estuarine circulations around the Changjiang estuary in the recent decade, (2000-2020). *Front. Mar. Sci.* 8. doi: 10.3389/fmars.2021.615929

Liu, K. K., Yan, W. J., Lee, H. J., Chao, S. Y., Gong, G. C., and Yeh, T. Y. (2015). Impacts of increasing dissolved inorganic nitrogen discharged from Changjiang on primary production and seafloor oxygen demand in the East China Sea from 1970 to 2002. *J. Mar. Syst.* 141, 200–217. doi: 10.1016/j.jmarsys.2014.07.022

Lü, X. G., Qiao, F. L., Xia, C. S., Wang, G. S., and Yuan, Y. L. (2010). Upwelling and surface cold patches in the Yellow Sea in summer: Effects of tidal mixing on the vertical circulation. *Continental Shelf Res.* 30 (6), 620–632. doi: 10.1016/j.csr.2009.09.002

Lü, X. G., Qiao, F. L., Xia, C. S., and Yuan, Y. L. (2007). Tidally induced upwelling off Yangtze River estuary and in Zhejiang coastal waters in summer. *Sci. China Ser. D-Earth Sci.* 50 (3), 462–473. doi: 10.1007/s11430-007-2050-0

Lü, X. G., Qiao, F. L., Xia, C. S., Zhu, J. R., and Yuan, Y. L. (2006). Upwelling off Yangtze River estuary in summer. *J. Geophys. Research-Oceans* 111 (C11), 19. doi: 10.1029/2005jc003250

Lui, H. K., Chen, C. T. A., Lee, J., Bai, Y., and He, X. Q. (2014). Looming hypoxia on outer shelves caused by reduced ventilation in the open oceans: Case study of the East China Sea. *Estuar. Coast. Shelf Sci.* 151, 355–360. doi: 10.1016/j.ecss.2014.08.010

Luo, Y. F., Shi, J., Guo, X. Y., Mao, X. Y., Yao, P., Zhao, B., et al. (2023). Yearly variations in nutrient supply in the East China sea due to the Zhejiang coastal upwelling and Kuroshio intrusion. *J. Geophys. Research-Oceans* 128 (4), 18. doi: 10.1029/2022jc019216

Meng, Q. C., Xuan, J. L., Zhang, W. Y., Zhou, F., Hao, Q., Zhao, Q., et al. (2020). Impact of submesoscale vertical advection on primary productivity in the Southern East China sea. *J. Geophys. Research-Biogeosci.* 125 (8), 21. doi: 10.1029/2019jg005540

Ning, X., Lin, C., Su, J., Liu, C., Hao, Q., and Le, F. (2011). Long-term changes of dissolved oxygen, hypoxia, and the responses of the ecosystems in the East China Sea from 1975 to 1995. *J. Oceanogr.* 67 (1), 59–75. doi: 10.1007/s10872-011-0006-7

Oschlies, A., Brandt, P., Stramma, L., and Schmidtko, S. (2018). Drivers and mechanisms of ocean deoxygenation. *Nat. Geosci.* 11 (7), 467–473. doi: 10.1038/s41561-018-0152-2

Oziel, L., Neukermans, G., Ardyna, M., Lancelot, C., Tison, J. L., Wassmann, P., et al. (2017). Role for Atlantic inflows and sea ice loss on shifting phytoplankton blooms in the Barents Sea. *J. Geophys. Research-Oceans* 122 (6), 5121–5139. doi: 10.1002/2016jc012582

Rabouille, C., Conley, D. J., Dai, M. H., Cai, W. J., Chen, C. T. A., Lansard, B., et al. (2008). Comparison of hypoxia among four river-dominated ocean margins: The Changjiang (Yangtze), Mississippi, Pearl, and Rhone rivers. *Continental Shelf Res.* 28 (12), 1527–1537. doi: 10.1016/j.csr.2008.01.020

Sathish, T., Kuttippurath, J., Purushothaman, A., Amal, K. S., Mohan, R., John, L., et al. (2023). Observed evidence for the impact of coastal currents on the recurrent Noctiluca scintillans blooms in the northwest Indian Ocean coast. *Mar. pollut. Bull.* 194 (Pt A), 115426. doi: 10.1016/j.marpolbul.2023.115426

Shchepetkin, A. F., and McWilliams, J. C. (2005). The regional oceanic modeling system (ROMS): a split-explicit, free-surface, topography-following-coordinate oceanic model. *Ocean Model.* 9 (4), 347–404. doi: 10.1016/j.ocemod.2004.08.002

Sun, X. H., Li, Z., Ding, X. Y., Ji, G. L., Wang, L., Gao, X. T., et al. (2022). Effects of algal blooms on phytoplankton composition and hypoxia in coastal waters of the Northern Yellow Sea, China. *Front. Mar. Sci.* 9. doi: 10.3389/fmars.2022.897418

Tian, D., Zhou, F., Zhang, W. Y., Zhang, H., Ma, X., and Guo, X. Y. (2022). Effects of dissolved oxygen and nutrients from the Kuroshio on hypoxia off the Changjiang River estuary. *J. Oceanol. Limnol.* 40 (2), 515–529. doi: 10.1007/s00343-021-0440-3

Tong, Y. D., Zhao, Y., Zhen, G. C., Chi, J., Liu, X. H., Lu, Y. R., et al. (2015). Nutrient loads flowing into coastal waters from the main rivers of Chin, (2006-2012). *Sci. Rep.* 5, 12. doi: 10.1038/srep16678

Wang, B., Chen, J. F., Jin, H. Y., Li, D. W., Gao, S. Q., Tian, S. C., et al. (2023). Subsurface oxygen minima regulated by remineralization and bottom flushing along 123 degrees E in the inner East China Sea. *Front. Mar. Sci.* 9. doi: 10.3389/fmars.2022.1081975

Wang, B. D. (2009). Hydromorphological mechanisms leading to hypoxia off the Changjiang estuary. *Mar. Environ. Res.* 67 (1), 53–58. doi: 10.1016/j.marenvres.2008.11.001

Wang, B. D., Wei, Q. S., Chen, J. F., and Xie, L. P. (2012). Annual cycle of hypoxia off the Changjiang (Yangtze River) Estuary. *Mar. Environ. Res.* 77, 1–5. doi: 10.1016/j.marenvres.2011.12.007

Wang, W., Yu, Z., Song, X., Wu, Z., Yuan, Y., Zhou, P., et al. (2016). The effect of Kuroshio Current on nitrate dynamics in the southern East China Sea revealed by nitrate isotopic composition. *J. Geophys. Research-Oceans* 121 (9), 7073–7087. doi: 10.1002/2016jc011882

Wei, H., He, Y. C., Li, Q. J., Liu, Z. Y., and Wang, H. T. (2007). Summer hypoxia adjacent to the Changjiang Estuary. *J. Mar. Syst.* 67 (3-4), 292–303. doi: 10.1016/j.jmarsys.2006.04.014

Wei, Q. S., Yao, P., Xu, B. C., Zhao, B., Ran, X. B., Zhao, Y. H., et al. (2021). Coastal upwelling combined with the river plume regulates hypoxia in the Changjiang estuary and adjacent inner East China sea shelf. *J. Geophys. Research-Oceans* 126 (11), 19. doi: 10.1029/2021jc017740

Wei, Q. S., Yu, Z. G., Wang, B. D., Wu, H., Sun, J. C., Zhang, X. L., et al. (2017). Offshore detachment of the Changjiang River plume and its ecological impacts in summer. *J. Oceanogr.* 73 (3), 277–294. doi: 10.1007/s10872-016-0402-0

Wu, T., and Wu, H. (2018). Tidal mixing sustains a bottom-trapped river plume and buoyant coastal current on an energetic continental shelf. *J. Geophys. Research-Oceans* 123 (11), 8026–8051. doi: 10.1029/2018jc014105

Xu, L. J., Yang, D. Z., Greenwood, J., Feng, X. R., Gao, G. D., Qi, J. F., et al. (2020). Riverine and oceanic nutrients govern different algal bloom domain near the changjiang estuary in summer. *J. Geophys. Research-Biogeosci.* 125 (10), 26. doi: 10.1029/2020jg005727

Yang, D. Z., Yin, B. S., Chai, F., Feng, X. R., Xue, H. J., Gao, G. D., et al. (2018). The onshore intrusion of Kuroshio subsurface water from February to July and a mechanism for the intrusion variation. *Prog. Oceanogr.* 167, 97–115. doi: 10.1016/j.pocean.2018.08.004

Yang, D. Z., Yin, B. S., Sun, J. C., and Zhang, Y. (2013). Numerical study on the origins and the forcing mechanism of the phosphate in upwelling areas off the coast of Zhejiang province, China in summer. *J. Mar. Syst.* 123, 1–18. doi: 10.1016/j.jmarsys.2013.04.002

Zhang, W. X. (2022a). Unexpected high indirect impacts of riverine organic matter to coastal deoxygenation. *Water Res.* 225, 14. doi: 10.1016/j.watres.2022.119180

Zhang, W. F., Alatalo, P., Crockford, T., Hirzel, A. J., Meyer, M. G., Oliver, H., et al. (2023). Cross-shelf exchange associated with a shelf-water streamer at the Mid-Atlantic Bight shelf edge. *Prog. Oceanogr.* 210, 19. doi: 10.1016/j.pocean.2022.102931

Zhang, J., Cowie, G., and Naqvi, S. W. A. (2013). Hypoxia in the changing marine environment. *Environ. Res. Lett.* 8 (1), 3. doi: 10.1088/1748-9326/8/1/015025

Zhang, W. X., Dunne, J. P., Wu, H., Zhou, F., and Huang, D. J. (2022b). Using timescales of deficit and residence to evaluate near-bottom dissolved oxygen variation in coastal seas. *J. Geophys. Research-Biogeosci.* 127 (1), 14. doi: 10.1029/2021jg006408

Zhang, H. Y., Fennel, K., Laurent, A., and Bian, C. W. (2020). A numerical model study of the main factors contributing to hypoxia and its interannual and short-term variability in the East China Sea. *Biogeosciences* 17 (22), 5745–5761. doi: 10.5194/bg-17-5745-2020

Zhang, W. F. G., and Gawarkiewicz, G. G. (2015). Dynamics of the direct intrusion of Gulf Stream ring water onto the Mid-Atlantic Bight shelf. *Geophys. Res. Lett.* 42 (18), 7687–7695. doi: 10.1002/2015gl065530

Zhang, J., Gilbert, D., Gooday, A. J., Levin, L., Naqvi, S. W. A., Middelburg, J. J., et al. (2010). Natural and human-induced hypoxia and consequences for coastal areas: synthesis and future development. *Biogeosciences* 7 (5), 1443–1467. doi: 10.5194/bg-7-1443-2010

Zhang, W. X., Hetland, R. D., DiMarco, S. F., and Fennel, K. (2015). Processes controlling mid-water column oxygen minima over the Texas-Louisiana shelf. *J. Geophys. Research-Oceans* 120 (4), 2800–2812. doi: 10.1002/2014jc010568

Zhang, J., Liu, S. M., Ren, J. L., Wu, Y., and Zhang, G. L. (2007). Nutrient gradients from the eutrophic Changjiang (Yangtze River) Estuary to the oligotrophic Kuroshio waters and re-evaluation of budgets for the East China Sea Shelf. *Prog. Oceanogr.* 74 (4), 449–478. doi: 10.1016/j.pocean.2007.04.019

Zhang, W. X., Moriarty, J. M., Wu, H., and Feng, Y. (2021). Response of bottom hypoxia off the Changjiang River Estuary to multiple factors: A numerical study. *Ocean Model.* 159, 13. doi: 10.1016/j.ocemod.2021.101751

Zhang, W. X., Wu, H., Hetland, R. D., and Zhu, Z. Y. (2019). On mechanisms controlling the seasonal hypoxia hot spots off the Changjiang river estuary. *J. Geophys. Research-Oceans* 124 (12), 8683–8700. doi: 10.1029/2019jc015322

Zhang, W. X., Wu, H., and Zhu, Z. Y. (2018). Transient hypoxia extent off Changjiang river estuary due to mobile Changjiang river plume. *J. Geophys. Research-Oceans* 123 (12), 9196–9211. doi: 10.1029/2018jc014596

Zhou, F., Chai, F., Huang, D. J., Wells, M., Ma, X., Meng, Q. C., et al. (2020). Coupling and decoupling of high biomass phytoplankton production and hypoxia in a highly dynamic coastal system: the Changjiang (Yangtze river) estuary. *Front. Mar. Sci.* 7. doi: 10.3389/fmars.2020.00259

Zhou, F., Chai, F., Huang, D. J., Xue, H. J., Chen, J. F., Xiu, P., et al. (2017). Investigation of hypoxia off the Changjiang Estuary using a coupled model of ROMS-CoSiNE. *Prog. Oceanogr.* 159, 237–254. doi: 10.1016/j.pocean.2017.10.008

Zhou, P., Song, X. X., Yuan, Y. Q., Wang, W. T., Chi, L. B., Cao, X. H., et al. (2018). Intrusion of the Kuroshio Subsurface Water in the southern East China Sea and its variation in 2014 and 2015 traced by dissolved inorganic iodine species. *Prog. Oceanogr.* 165, 287–298. doi: 10.1016/j.pocean.2018.06.011

Zhu, J. R. (2003). Dynamic mechanism of the upwelling on the west side of the submerged river valley off the Changjiang mouth in summertime. *Chin. Sci. Bull.* 48 (24), 2754–2758. doi: 10.1360/03wd0179

Zhu, Z. Y., Wu, H., Liu, S. M., Wu, Y., Huang, D. J., Zhang, J., et al. (2017). Hypoxia off the Changjiang (Yangtze River) estuary and in the adjacent East China Sea: Quantitative approaches to estimating the tidal impact and nutrient regeneration. *Mar. pollut. Bull.* 125 (1-2), 103–114. doi: 10.1016/j.marpolbul.2017.07.029

Zhu, Z. Y., Zhang, J., Wu, Y., Zhang, Y. Y., Lin, J., and Liu, S. M. (2011). Hypoxia off the Changjiang (Yangtze River) Estuary: Oxygen depletion and organic matter decomposition. *Mar. Chem.* 125 (1-4), 108–116. doi: 10.1016/j.marchem.2011.03.005